Journal of Magnetism and Magnetic Materials 421 (2017) 177–183

Contents lists available at ScienceDirect

Journal of Magnetism and Magnetic Materials

journal homepage: www.elsevier.com/locate/jmmm

Microemulsion synthesis and magnetic properties of $Fe_xNi_{(1-x)}$ alloy nanoparticles

H. Beygi *, A. Babakhani

Department of Materials Science and Metallurgical Engineering, Engineering Faculty, Ferdowsi University of Mashhad, Mashhad, Iran

ARTICLE INFO

Article history:
Received 25 December 2015
Received in revised form
15 July 2016
Accepted 31 July 2016

Keywords:
Alloy nanoparticles
Microemulsion
Co-surfactant
Thermal properties
Superparamagnetic

ABSTRACT

This paper investigates synthesis of $Fe_xNi_{(1-x)}$ bimetallic nanoparticles by microemulsion method. Through studying the mechanism of nanoparticles formation, it is indicated that synthesis of nanoparticles took placed by simultaneous reduction of metal ions and so nanoparticles structure is homogeneous alloy. $Fe_xNi_{(1-x)}$ nanoparticles with different sizes, morphologies and compositions were synthesized by changing the microemulsion parameters such as water/surfactant/oil ratio, presence of co-surfactant and $NiCl_2 \cdot 6H_2O$ to $FeCl_2 \cdot 4H_2O$ molar ratio. Synthesized nanoparticles were characterized by transmission electron microscopy, particle size analysis, X-ray diffraction, atomic absorption and thermogravimetric analyses. The results indicated that, presence of butanol as co-surfactant led to chain-like arrangement of nanoparticles. Also, finer nanoparticles were synthesized by decreasing the amount of oil and water and increasing the amount of CTAB. The results of vibrating sample magnetometer suggested that magnetic properties of $Fe_xNi_{(1-x)}$ alloy nanoparticles were affected by composition, size and morphology of the particles. Spherical and chain-like $Fe_xNi_{(1-x)}$ alloy nanoparticles were superparamagnetic and ferromagnetic, respectively. Furthermore, higher iron in the composition of nanoparticles increases the magnetic properties.

© 2016 Elsevier B.V. All rights reserved.

1. Introduction

Nickel-iron alloys are considered for many applications in new and advanced industries due to their special magnetic properties. In such applications, magnetic properties are highly dependent on the chemical composition and ratio of elements in the alloy. An interesting nickel-iron alloy is $Fe_xNi_{(1-x)}$, while $x=20$–50 wt%. This alloy that called *permalloy* due to its high magnetic permeability has also high magnetic saturation and curie temperature [1,2]. Because of considerable magnetic properties, permalloy is used for many applications such as magnetic resonance imaging (MRI), sensors, recording heads, electromagnetic shielding and absorbing materials [3–5].

In the case of such magnetic alloys, changes in the size and shape of the particles can also cause various magnetic properties [1,5,6]. Decreasing the particle size to nanoscale dimensions leads to variations in magnetic properties [1,6]. Magnetic nanoparticles are particles with dimensions less than 100 nm that present size dependent magnetic properties according to two mechanisms of finite-size effect (for example, from the quantum confinement of the electrons) and surface effect (related to the symmetry breaking of the crystal structure at the boundary of each particle) [7]. Furthermore, according to *shape anisotropy* effect, different morphologies can magnetize the particles in specific directions, so lead to various magnetic properties [1].

Among different methods reported for synthesis of magnetic nanoparticles, *water in oil microemulsion* method has great tendency for the synthesis of particles with controllable sizes and morphologies [8,9]. In this method, nanoparticles are synthesized in small reactors called *reverse micelles;* numerous water droplets distributed in an organic phase by the means of a surface active agent (surfactant). Here, size and morphology of synthesized particles are proportional to the size and shape of water droplets. Therefore, particles with different sizes and morphologies can be synthesized by controlling the parameters of microemulsion method [8]. The most important parameters of microemulsion method can describe as follows:

a) parameters of micellar structure; such as type of organic phase and surfactant, aqueous/organic/surfactant ratio and benefits of co-surfactants to control the shape of water droplets,
b) parameters of chemical composition or type and concentration of the reactants,
c) process parameters such as temperature, pH, mixing method, rate of mixing, stirring method and stirring time [8–11].

* Corresponding author.
E-mail addresses: hossein.beygi@stu-mail.um.ac.ir, beygi@alumni.ubc.ca (H. Beygi).

http://dx.doi.org/10.1016/j.jmmm.2016.07.071
0304-8853/© 2016 Elsevier B.V. All rights reserved.

In the only report about synthesis of FeNi particles by microemulsion method, Ban et al. [10] studied synthesis of nano-sized $Fe_{0.2}Ni_{0.8}$ particles through reduction of metal salts by sodium borohydride ($NaBH_4$). Synthesized nanoparticles had primitive cubic (PC) lattice and their structure changed to body-centered cubic (BCC) after heat treatment at 700 °C. Reflecting the influence of nano-dimensions, magnetization of such nanoparticles was much lower than that of the bulk material [10].

Dependence of magnetic properties to composition, size and morphology of particles also studied for FeNi particles synthesized by other methods. For example, magnetic properties of $Fe_{100-x}Ni_x$ alloys produced by mechanical alloying affected by chemical composition [12,13]. Maxwell-Garnett and Bruggeman theories were also investigated the effects of particle size on the magnetic behavior of FeNi micro-particles [14]. Different magnetic properties were also reported for FeNi particles with different morphologies of chain-like [5,15], nanowires and nanotubes [16], leaf-like [17], flower-like [18] and triangular [19].

Present study aims to study magnetic properties of FeNi particles regarding to the composition, size and morphology of the particles. For this purpose, various microemulsion compounds are used to synthesis particles with different morphologies. The effects of water/surfactant/oil ratios are investigated on the particle size, and nanoparticles with different compositions are synthesized by changing the reaction stoichiometry. The research results are important because illustrate the capability of microemulsion method for synthesis of nanoparticles with various compositions, sizes and morphologies. Other sides, interesting magnetic properties of $Fe_xNi_{(1-x)}$ nanoparticles can be provided by controlling the synthesis parameters.

2. Experimental

2.1. Materials

Nickel chloride ($NiCl_2 \cdot 6H_2O$, JHD) and iron chloride ($FeCl_2 \cdot 4H_2O$, Merck) as the source of nickel and iron, hydrazine ($N_2H_4 \cdot H_2O$, Scharlau) as the reducing agent, sodium hydroxide (NaOH, Merck) for controlling the pH, deionized water, 1-hexanol ($C_6H_{14}O$, Sigma) and octane (C_8H_{18}, Scharlau) as the organic phases of microemulsion, CTAB ($C_{19}H_{42}BrN$, Suvchem) and *n*-butanol (C_4H_9OH, Flucka) as surfactant and co-surfactant, respectively.

2.2. Synthesis method

Two microemulsions with a similar oil/surfactant/water ratio were prepared. The water in the first microemulsion was aqueous solution of $N_2H_4 \cdot H_2O$ (5 M), while NaOH was added to increase its pH to 12. In the second one, the water was aqueous solution of metal chlorides (0.05 M). Here, three different molar ratios of $NiCl_2 \cdot 6H_2O$ and $FeCl_2 \cdot 4H_2O$ were used for synthesis of $Fe_{0.1}Ni_{0.9}$, $Fe_{0.2}Ni_{0.8}$ and $Fe_{0.3}Ni_{0.7}$ bimetallic particles. Bimetallic particles were synthesized one hour after mixing the two microemulsions at 70 °C, and according to the following reactions:

$$7NiCl_2 \cdot 6H_2O + 3\ FeCl_2 \cdot 4H_2O + 5\ N_2H_4 \cdot H2O + 20NaOH \rightarrow 10Fe_{0.3}Ni_{0.7} + 5\ N_2 + 79H_2O + 20\ NaCl \quad (1)$$

$$8NiCl_2 \cdot 6H_2O + 2\ FeCl_2 \cdot 4H_2O + 5\ N_2H_4 \cdot H2O + 20\ NaOH \rightarrow 10\ Fe_{0.2}Ni_{0.8} + 5\ N_2 + 81H_2O + 20\ NaCl \quad (2)$$

$$9NiCl_2 \cdot 6H_2O + 1\ FeCl_2 \cdot 4H_2O + 5\ N_2H_4 \cdot H2O + 20\ NaOH \rightarrow 10\ Fe_{0.1}Ni_{0.9} + 5\ N_2 + 83H_2O + 20\ NaCl \quad (3)$$

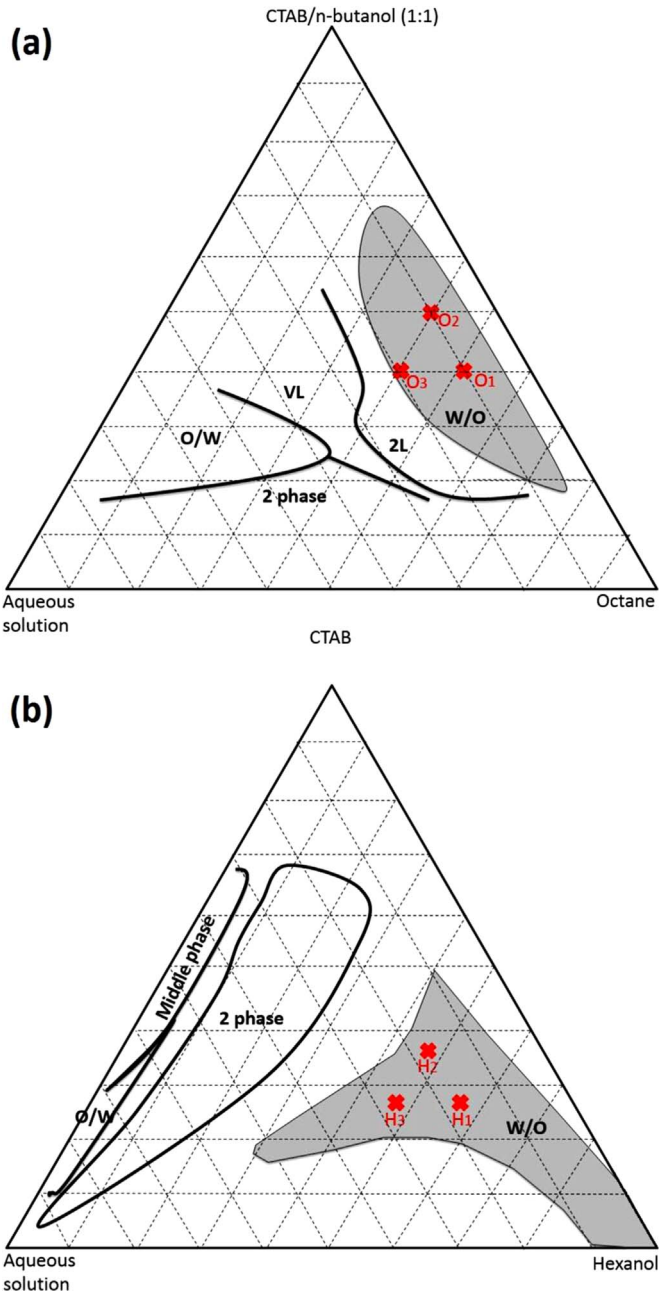

Fig. 1. (a) Ternary diagram of octane/CTAB+butanol/water [20], (b) Ternary diagram of hexanol/CTAB/water [21].

2.3. Design of experiments

In this study, two microemulsion systems of octane/CTAB+butanol/water and hexanol/CTAB/water (with various oil/surfactant/water ratios) are selected to synthesis nanoparticles with different sizes and morphologies. The compositions of both microemulsion systems are chosen in such a way that stable reverse micelles can be formed according to the ternary diagrams of Fig. 1. Selected microemulsion compositions and array of designed experiments present in Table 1. First, synthesis of $Fe_{0.2}Ni_{0.8}$ particles is studied; experiments No. 1 to 3 in the octane/CTAB+butanol/water microemulsion system, and experiments No. 4 to 6 in the microemulsion system of hexanol/CTAB/water. Subsequently, the microemulsion composition that leads to synthesis of the finest nanoparticles is used for synthesis of $Fe_{0.3}Ni_{0.7}$ and $Fe_{0.1}Ni_{0.9}$ bimetallic nanoparticles.

Table 1
Microemulsion compositions and array of designed experiments.

No.	Microemulsion composition	Feeding solution $FeCl_2$:$NiCl_2$
1	O1 (Octane/CTAB+Butanol/Water=50/40/10)	2:8
2	O2 (Octane/CTAB+Butanol/Water=40/50/10)	2:8
3	O3 (Octane/CTAB+Butanol/Water=40/40/20)	2:8
4	H1 (Hexanol/CTAB/Water=56/26/18)	2:8
5	H2 (Hexanol/CTAB/Water=46/36/18)	2:8
6	H3 (Hexanol/CTAB/Water=46/26/28)	2:8
7	H2 (Hexanol/CTAB/Water=46/36/18)	3:7
8	H2 (Hexanol/CTAB/Water=46/36/18)	1:9

2.4. Characterization methods

Mean size of the synthesized bimetallic particles was measured using a particle size analyzer (PSA, Fritsch A22). Morphology of the nanoparticles was studied by transmission electron microscopy (TEM, LEO 912 AB). In addition, phase identification of synthesized particles was performed with X-ray diffractometer (XRD, Philips X'Pert diffractometer) using Cu-Kα radiation (λ=0.15406 nm). Atomic absorption spectroscopy (AAS, Shimadzu AA-670) was used to study the chemical composition of particles. In order to investigate particles oxidation, thermogravimetric analysis (TGA, Bahr STA 503) was performed with a heating rate of 10 °C/min at air atmosphere. Magnetic properties of synthesized particles also measured using vibrating sample magnetometer test (VSM) at room temperature.

Samples for XRD, AAS, TGA and VSM were prepared after three steps of centrifugation-assisted separation of particles, washing with ethanol and drying the particles at room temperature.

3. Results and discussion

3.1. Effects of microemulsion parameters on the size and morphology of particles

Fig. 2 shows the TEM images of iron–nickel particles synthesized by different microemulsion systems. As seen, particles synthesized in hexanol/CTAB/water microemulsion system (experiments No. 5) have spherical shape with mean particle size of 7 nm. On the other side, chain-like morphologies resulting from aggregation of much larger spherical particles synthesized in the octane/CTAB+butanol/water microemulsion systems (experiments No. 2 and 3). It is noteworthy that, the chain structures keep unbroken under ultrasonication, indicating the structures of as-prepared iron–nickel chains are stable.

The formation of chain-like arrangement of nanoparticles can be related to the shape of micelles, that generally affected by the type of microemulsion components. In this regard, presence of *n*-butanol with short hydrophobic chain and terminal hydroxyl group, enhances the interaction with surfactant at the water/oil interface and affects the interface energy and its curvature. The interface curvature becomes more, if longer-chain co-surfactant uses [22,23]. This variation in the interface curvature causes the water in oil droplets or synthesis reactors change to stretched-shape. It was reported that synthesis in such microemulsion system leads to the growth of initially nuclei in the stretched reactors and formation of needle or rod-shaped morphologies [10,11,23]. However, the nucleation step seems to be dominant in the present case, so different nuclei are formed within the reactors, and they are connected by subsequent growth step. Our further observations about the synthesis process confirm the rapid nucleation and slow growth of nanoparticles. Connection of neighboring particles and formation of the chain-like structures can also be justified due to physical adsorption of surfactants on the particles surfaces. Adsorbed CTAB on the surface of particles can partially compensate the negative surface charge, leading to an anisotropic distribution of the residual surface charges. This extrinsic electric dipole formation is responsible for the linear organization of the particles into chains [15].

Particle size measurement of $Fe_{0.2}Ni_{0.8}$ nanoparticles synthesized in hexanol/CTAB/water microemulsion system (experiments No. 4, 5 and 6) confirms that spherical nanoparticles with different sizes can be synthesized by changing the water/oil/surfactant ratios (Fig. 3a). Here, the experiments were designed in such a way that by fixing one value, variation in the ratio of two other components can be investigated. For example, H1 and H2 experiments demonstrate that in a fixed amount of water, size of nanoparticles decreases by increasing the CTAB/hexanol ratio. Another side, in experiments with the fixed amount of hexanol (H2 and H3), size of the iron–nickel nanoparticles increases at higher water to surfactant ratios. Increasing the water amount in the microemulsion

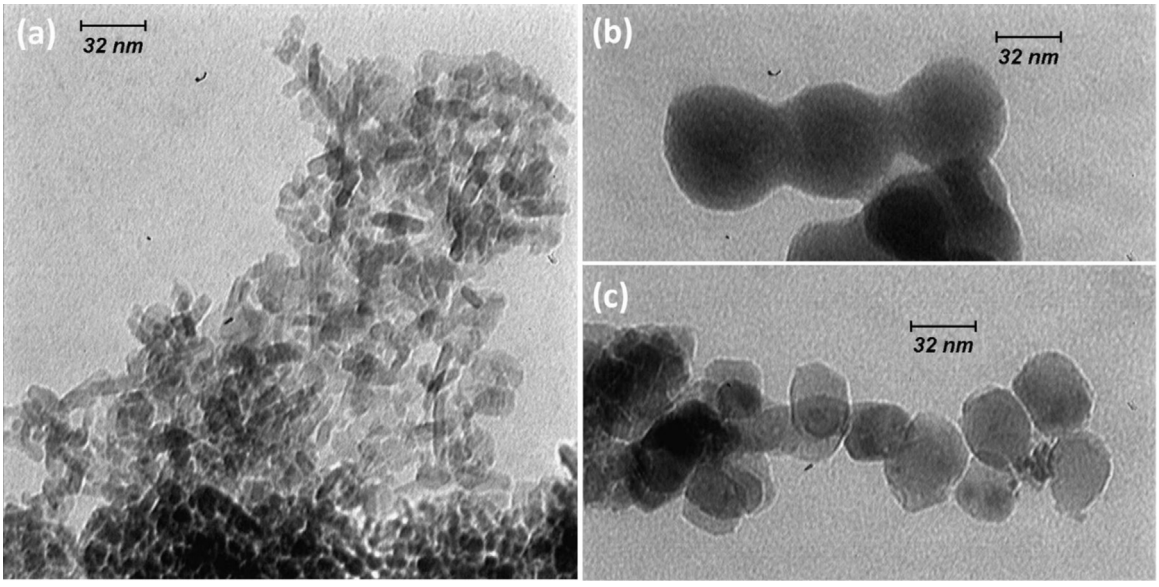

Fig. 2. TEM micrographs of nanoparticles synthesized in experiments: (a) No. 5, (b) No. 2, (c) No. 3.

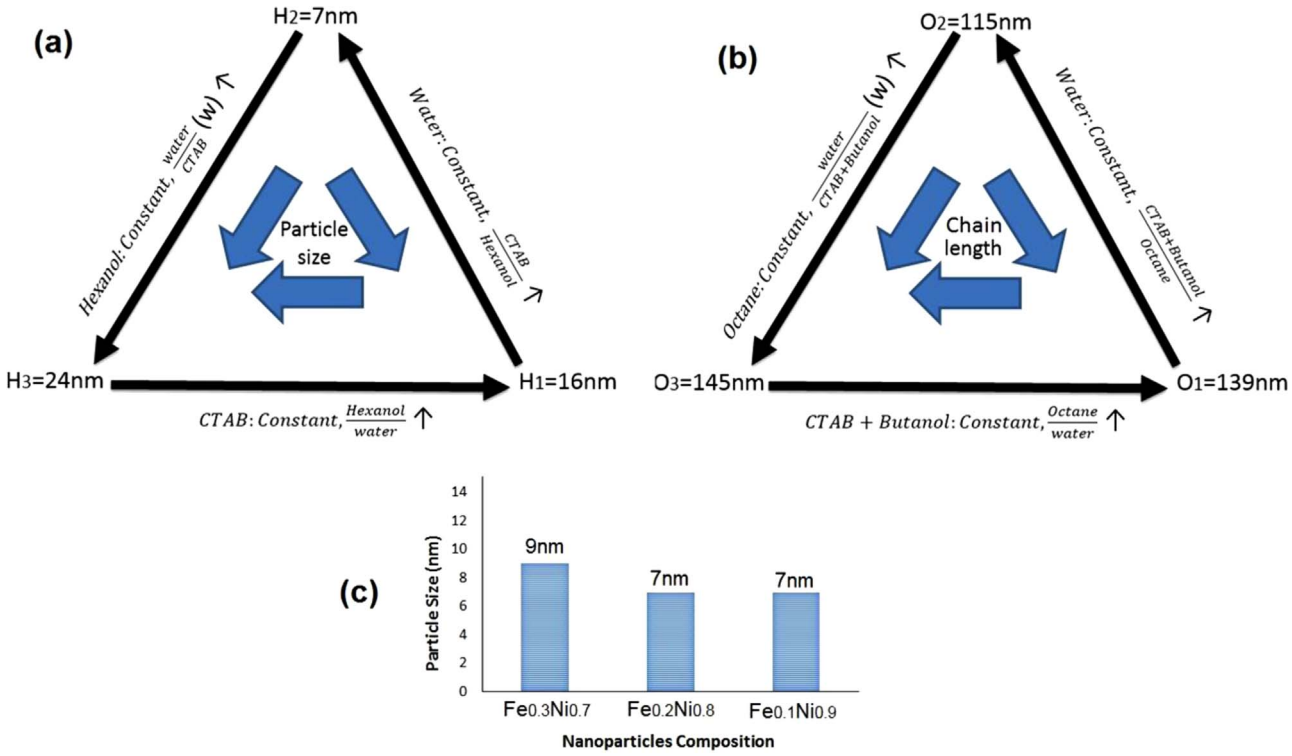

Fig. 3. Size of particles synthesized in: (a) hexanol/CTAB/water microemulsions (experiments No. 4, 5 and 6), (b) octane/CTAB+butanol/water microemulsions (experiments No. 1, 2 and 3), (c) hexanol/CTAB/water =46/36/18 microemulsion and different nanoparticles composition (experiments No. 5, 7 and 8).

system leads to preparation of bigger micelles, so synthesis of bigger nanoparticles. The same argument can be explained particle size reduction by increasing the hexanol to water ratios at the constant surfactant values (experiments H3 and H1).

The results of Fig. 3b show the same variations in the length of $Fe_{0.2}Ni_{0.8}$ chains synthesized in octane/CTAB+butanol/water microemulsion system. As acceptable logics, these observations can be extended to other water in oil microemulsion systems that lower amount of oil and water and higher CTAB amount decreased the micelles sizes as well as the size of synthesized particles. Since water droplets are stretched in this microemulsion system, more nuclei can be formed in the larger droplets. For example, a chain of particles synthesized in experiment No. 2 (Fig. 2b) has about 115 nm long and consists of three spherical particles with mean diameter of 40 nm. Moreover, mean chain length of 145 nm was measured for structures synthesized in experiment No. 3 (Fig. 2c) and these chains were assembled from more particles with mean diameter of about 30 nm.

Iron–nickel nanoparticles with different chemical compositions were also synthesized in the microemulsion system of hexanol/CTAB/water=46/36/18 (experiments No. 5, 7 and 8). In these experiments, three $NiCl_2 \cdot 6H_2O$ to $FeCl_2 \cdot 4H_2O$ molar ratios were used to synthesis different nanoparticles (according to reactions 1, 2 and 3). According to Fig. 3c, size of the synthesized nanoparticles is same, indicating chemical composition has a low effect on the particle size.

3.2. Mechanism of alloy nanoparticles formation

Elemental iron/nickel ratios of nanoparticles synthesized by experiments No. 5, 7 and 8 were measured by atomic absorption and the results presented in Table 2. As mentioned, three different $NiCl_2 \cdot 6H_2O$ to $FeCl_2 \cdot 4H_2O$ molar ratios were used for synthesis of $Fe_xNi_{(1-x)}$ (x=0.1, 0.2, 0.3) bimetallic nanoparticles. It can be seen

Table 2
Atomic absorption results for synthesized nanoparticles with different compositions.

Sample	Feeding solution $FeCl_2$:$NiCl_2$	Elemental ratio by AAS Fe:Ni
5	2:8	18.33:81.67
7	3:7	28.36:71.64
8	1:9	9.18:90.82

that obtained percentages from the atomic absorption analysis match well with the initial molar ratios of chlorides, so synthesis of bimetallic nanoparticles by desired elemental ratios were done successfully.

This good match between the molar ratios of chlorides and composition of bimetallic nanoparticles can be explained by two possibilities; both the iron and nickel ions have been completely reduced at the synthesis time, or two ions have been simultaneously reduced even they were not completely reduced. In order to study the first hypothesis, percentage of reaction progress was calculated by measuring the weight of synthesized particles at different times. As seen in Fig. 4, the reaction progress rate is high at the first times after mixing two microemulsions, and then the reaction rate decreases. In other words, the reduction of metal ions (Eqs. (1)–(3)) began immediately after mixing two microemulsions, but it slowed by time and so these reactions did not complete at the end of synthesis time. Since hydrazine is added much higher than stoichiometry, the sharp decrease in the reaction rate cannot be related to the consumption of reactants or reaction stability. Further studies indicate a drop in the bath pH at the first stages of synthesis process. This result is quite acceptable according to the reaction stoichiometries, because OH^- ions are consumed by the reaction products. These observations demonstrate that the first hypothesis about completely reduction of iron and nickel ions at the synthesis time is not true. According to the

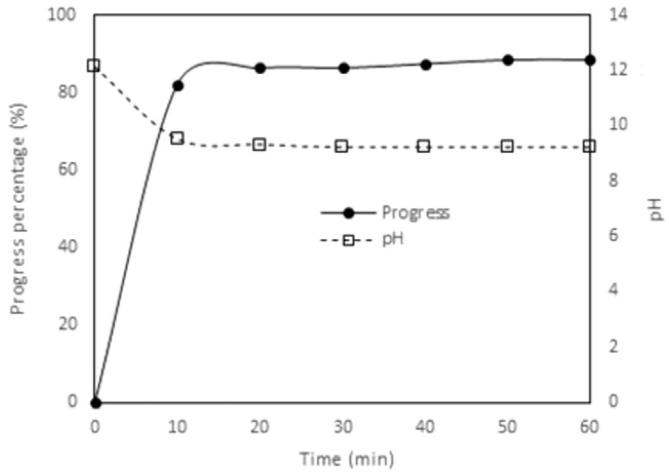

Fig. 4. Variation of pH and reaction progress percentage at different synthesis times.

good match between the molar ratios of chlorides and composition of bimetallic nanoparticles, it is likely that two ions simultaneously reduced. This hypothesis has a significant effect on the structure of nanoparticles.

The structure of synthesized $Fe_xNi_{(1-x)}$ bimetallic nanoparticles will be different according to the reduction mechanism of iron and nickel. In the presence of suitable stabilization strategy, successive reduction of two metal ions leads to synthesis of core–shell structures. In contrast, if the synthesis takes place by simultaneous reduction of metal ions, depending to reduction conditions (such as reduction potential, rates of nucleation and growth, concentration and ratio of ions) particles may have structures between the core–shell and homogeneous alloy [24]. In the case of synthesis of $Fe_xNi_{(1-x)}$ bimetallic nanoparticles by the presented method, the redox potentials of the chemicals are as follows:

$$Fe^{2+} + 2e^- \rightarrow FeE^\circ = -0.44\ V \quad (4)$$

$$Ni^{2+} + 2e^- \rightarrow NiE^\circ = -0.25\ V \quad (5)$$

$$N_2H_4 + 4OH^- \rightarrow N_2 + H_2O + 4e^- E^\circ = 1.16\ V \quad (6)$$

Since iron and nickel ions have different redox potentials, synthesis of nanoparticles with core–shell structure is expected. However, because high potential hydrazine is added much higher than stoichiometry, metal ions may not have a tough competition for reduction, and both the ions are reduced simultaneously. Higher nickel ions also help the simultaneous reduction. As a result, synthesis of $Fe_xNi_{(1-x)}$ bimetallic nanoparticles took placed by simultaneous reduction of metal ions and so nanoparticles structure is homogeneous alloy.

Fig. 5 shows the X-ray diffraction pattern of nanoparticles synthesized by experiment No. 5. According to the database of the international center of diffraction data (ICDD), presented pattern has a perfect match with 00-012-0736 ICDD reference pattern of (Ni, Fe) solid solution. In this pattern, the observed peaks at 43.92, 51.19 and 75.44 angles relate to (111), (200) and (220) planes, respectively. It should be noted that peaks of mentioned planes for pure nickel with the FCC lattice are at 44.50, 51.85 and 76.38 angles, respectively. It can be concluded that by diffusion of iron into the Ni lattice and subsequent lattice expansion, the angles are shifted slightly to the left. These observations prove the formation of $Fe_xNi_{(1-x)}$ alloy nanoparticles.

3.3. Oxidation of $Fe_xNi_{(1-x)}$ alloy nanoparticles

X-ray diffraction pattern of nanoparticles (Fig. 5) only indicates the (Ni, Fe) solid solution peaks, nor any peaks of reactants or unwanted martials. This good indication shows that nickel oxides and hydroxides were not produced during the synthesis process. Especially, nickel oxidation was likely regarding to the high temperature reactions in aqueous environment. No nickel oxidation can be justified by the reactor protection viewpoint. In other words, in this method water droplets or synthesis reactors are protected from the air atmosphere by the oily matrix. In addition, the synthesis process was performed in N_2 protective atmosphere that produced by reaction (2).

To study the oxidation of iron–nickel nanoparticles at higher temperatures, the results of thermogravimetric analysis (TGA) as well as differential thermogravimetric curve (DTG) are presented in Fig. 6. As can be seen, nanoparticles weight increases gradually by temperature due to the oxygen absorption by iron and nickel at elevated temperatures. Below 300 °C, a slight weight gain indicates poor oxidation of nanoparticles at lower temperatures. This temperature can be considered as the starting oxidation temperature of $Fe_{0.2}Ni_{0.8}$ nanoparticles, which is much lower than that of bulk materials [25]. Increase in the slop of DTG curve indicates accelerated oxidation from 300 °C and fastest oxidation rate at 680 °C. The nanoparticles oxidation rate reduces gradually, and no other weight gain observes above 1100 °C. The total weight gain observed in the TGA curve is about 33% at this temperature. According to the theatrical weight gain causing by ideally oxidation of iron–nickel nanoparticles to FeO and NiO, it can be concluded that all the nanoparticles oxidized at this temperature.

3.4. Magnetic properties of $Fe_xNi_{(1-x)}$ alloy nanoparticles

The magnetization-magnetic field loops of $Fe_xNi_{(1-x)}$ alloy nanoparticles with different compositions and morphologies are presented in Fig. 7. First, hysteresis loops of nanoparticles with the same composition of $Fe_{0.2}Ni_{0.8}$ are compared to investigate the effect of particles morphologies on the magnetic properties. In the case of spherical nanoparticles with mean size of 7 nm, the hysteresis loop is so narrow and values of saturation magnetization (M_s), remanent magnetization (M_r), and the coercivity (H_c) are

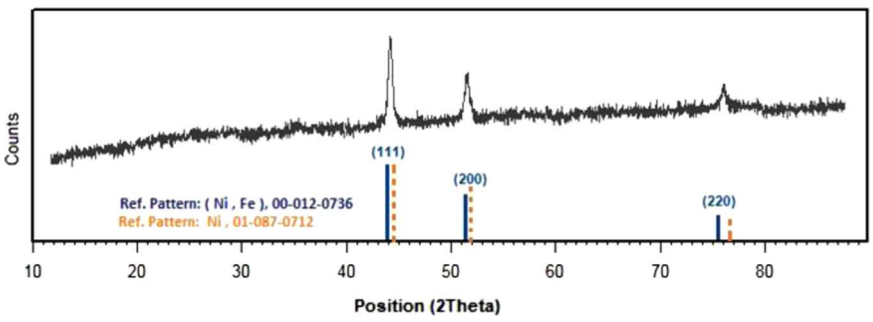

Fig. 5. X-ray diffraction pattern of synthesized $Fe_xNi_{(1-x)}$ nanoparticles by experiment. No. 5.

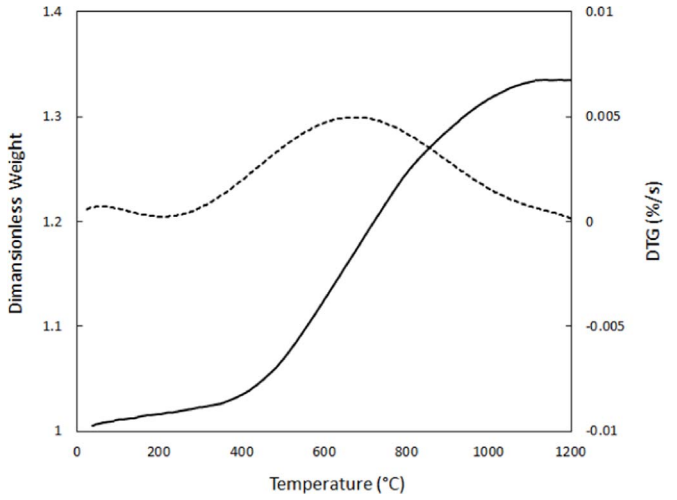

Fig. 6. Thermogravimetric (TG) and differential thermogravimetric (DTG) curves of $Fe_{0.2}Ni_{0.8}$ nanoparticles.

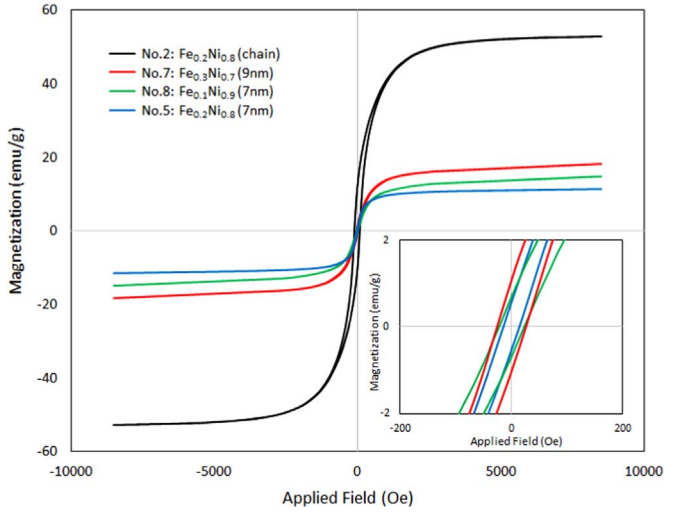

Fig. 7. Magnetization-magnetic field loops of $Fe_xNi_{(1-x)}$ particles synthesized by experiments No. 2, 5, 7 and 8 (25 °C).

11.4 emu/g, 0.54 emu/g and 15.2 Oe, respectively. Spherical $Fe_{0.2}Ni_{0.8}$ nanoparticles with such small size seem to be a kind of single domain, so the thermal fluctuations energy can overcome the anisotropic energy, and nanoparticles find the superparamagnetic properties. The other side, values of M_s, M_r and H_c for chain-like morphologies increased to 52.8 emu/g, 11.2 emu/g and 88.2 Oe, respectively. In this case, increased size and shape anisotropy lead to ferromagnetic properties of particles. It is also reported that higher aspect ratio of chains of magnetic particles may results in a much larger dipole moment and higher coercivity [15].

Effect of chemical composition on the magnetic behavior of $Fe_xNi_{(1-x)}$ alloy nanoparticles can also be investigated by comparing the hysteresis loops of nanoparticles with different iron to nickel ratios. Curves of 5, 7 and 8 in Fig. 7, show the magnetic behavior of iron–nickel particles with different compositions, but same sizes and morphologies. The lack of hysteresis loop for all three samples suggests the superparamagnetic behavior. The general trend in variation of M_s, M_r and H_c indicates that higher amount of iron increases the magnetic properties of $Fe_xNi_{(1-x)}$ alloy nanoparticles. It is expected that composition may has a slight effect on the magnetic properties of nanoparticles due to the same magnetic behavior of nickel and iron. However, variations in magnetic properties of such nanoparticles can be explained by other factors such as changes in the structure and atomic arrangement of particles, disorder degree in the structure of nanoparticles and also nanoparticle size variations [1,10,11].

4. Conclusions

1. Particles synthesized in hexanol/CTAB/water microemulsion system have spherical shape with mean size of 7 nm. Presence of butanol as co-surfactant, stretches the oil-water interfaces and creates chain-like morphologies.
2. Size of synthesized particles decreases at lower amount of oil and water and higher CTAB amounts.
3. Synthesis of $Fe_xNi_{(1-x)}$ bimetallic nanoparticles takes place by simultaneous reduction of metal ions and so nanoparticles structure is homogeneous alloy.
4. Spherical and chain-like $Fe_xNi_{(1-x)}$ alloy nanoparticles were superparamagnetic and ferromagnetic, respectively. Also, spherical $Fe_xNi_{(1-x)}$ nanoparticles with higher x had increased magnetic properties.

Acknowledgment

The authors wish to express appreciation to Research Deputy of Ferdowsi University of Mashhad for supporting this project by Grant no.: 2/27806-18/4/92.

References

[1] B.D. Cullity, C.D. Graham, Introduction to Magnetic Materials, 2, John Wiley & Sons, 2011, ISBN: 1118211499, 9781118211496 https://books.google.ca/books?id=fh_F0G9KuSgC&dq=Introduction+to+Magnetic+Materials&source=gbs_navlinks_s.
[2] X. Lu, G. Huo, X. Liu, G. Liang, Z. Han, X. Song, Hierarchical $FeNi_3$ assemblies with caltrop-like architectures: synthesis, formation mechanism and magnetic properties, CrystEngComm 14 (2012) 5622–5626.
[3] H. Beygi, S. Sajjadi, M. Zare, Synthesis and characterization of permalloy-reinforced Al_2O_3 nanocomposite powders by mechanical alloying, Int. J. Adv. Manuf. Technol. 70 (2014) 1653–1659.
[4] H. Beygi, M. Zare, S. Sajjadi, Fabrication of FeNi–Al_2O_3 nanocomposites and optimization of mechanical properties using Taguchi method, Powder Technol. 232 (2012) 49–57.
[5] G. Cheng, Fabrication and characterisation of iron-nickel chain-like fibres via simple solvothermal approach, Mater. Res. Innov. 19 (2015) 69–72.
[6] X. Li, A. Chiba, S. Takahashi, Preparation and magnetic properties of ultrafine particles of Fe•Ni alloys, J. Magn. Magn. Mater. 170 (1997) 339–345.
[7] A.H. Lu, Ee.L. Salabas, F. Schüth, Magnetic nanoparticles: synthesis, protection, functionalization, and application, Angew. Chem. Int. Ed. 46 (2007) 1222–1244.
[8] I. Capek, Preparation of metal nanoparticles in water-in-oil (w/o) microemulsions, Adv. Colloid Interface Sci. 110 (2004) 49–74.
[9] V. Uskoković, M. Drofenik, Synthesis of materials within reverse micelles, Surf. Rev. Lett. 12 (2005) 239–277.
[10] I. Ban, M. Drofenik, D. Makovec, The synthesis of iron–nickel alloy nanoparticles using a reverse micelle technique, J. Magn. Magn. Mater. 307 (2006) 250–256.
[11] D.-E. Zhang, X.-M. Ni, X.-J. Zhang, H.-G. Zheng, Synthesis and characterization of Ni–Co needle-like alloys in water-in-oil microemulsion, J. Magn. Magn. Mater. 302 (2006) 290–293.
[12] Y.V. Baldokhin, V.V. Tcherdyntsev, S.D. Kaloshkin, G.A. Kochetov, Y.A. Pustov, Transformations and fine magnetic structure of mechanically alloyed Fe–Ni alloys, J. Magn. Magn. Mater. 203 (1999) 313–315.
[13] C. Kuhrt, L. Schultz, Formation and magnetic properties of nanocrystalline mechanically alloyed Fe-Co and Fe-Ni, J. Appl. Phys. 73 (1993) 6588–6590.
[14] A. Berthault, D. Rousselle, G. Zerah, Magnetic properties of permalloy microparticles, J. Magn. Magn. Mater. 112 (1992) 477–480.
[15] X. Lu, Q. Liu, G. Huo, G. Liang, Q. Sun, X. Song, CTAB-mediated synthesis of iron–nickel alloy nanochains and their magnetic properties, Colloids Surf. A: Physicochem. Eng. Asp. 407 (2012) 23–28.
[16] S. Xue, M. Li, Y. Wang, X. Xu, Electrochemically synthesized binary alloy FeNi

nanorod and nanotube arrays in polycarbonate membranes, Thin Solid Films 517 (2009) 5922–5926.
[17] Y. Cao, S.G. Ai, J. Zhang, N. Gu, S. Hu, Template-free synthesis and characterization of leaf-like Fe-Ni microstructures, 2012.
[18] L. Liu, J. Guan, W. Shi, Z. Sun, J. Zhao, Facile synthesis and growth mechanism of flowerlike Ni– Fe alloy nanostructures, J. Phys. Chem. C 114 (2010) 13565–13570.
[19] D. Niu, X. Zou, J. Wu, Y. Xu, Anisotropic magnetization reversal in 30 nm triangular FeNi dots, Appl. Phys. Lett. 94 (2009) 072501.
[20] J.B. Nagy, Multinuclear NMR characterization of microemulsions: preparation of monodisperse colloidal metal boride particles, Colloids Surf. 35 (1989) 201–220.
[21] S.I. Ahmad, S. Friberg, Catalysis in micellar and liquid-crystalline phases. I. System water-hexadecyltrimethylammonium bromide-hexanol, J. Am. Chem. Soc. 94 (1972) 5196–5199.
[22] T. Charinpanitkul, A. Chanagul, J. Dutta, U. Rungsardthong, W. Tanthapanichakoon, Effects of cosurfactant on ZnS nanoparticle synthesis in microemulsion, Sci. Technol. Adv. Mater. 6 (2005) 266–271.
[23] R. Ranjan, S. Vaidya, P. Thaplyal, M. Qamar, J. Ahmed, A.K. Ganguli, Controlling the size, morphology, and aspect ratio of nanostructures using reverse micelles: a case study of copper oxalate monohydrate, Langmuir 25 (2009) 6469–6475.
[24] M.-L. Wu, L.-B. Lai, Synthesis of Pt/Ag bimetallic nanoparticles in water-in-oil microemulsions, Colloids Surf. A: Physicochem. Eng. Asp. 244 (2004) 149–157.
[25] P. Song, D. Wen, Z. Guo, T. Korakianitis, Oxidation investigation of nickel nanoparticles, Phys. Chem. Chem. Phys. 10 (2008) 5057–5065.